

Supplementary methods

EOF analysis of the satellite altimetry data. The Sea Level Anomaly (SLA) data are organized as an array with a value, $h(x_i, y_i, t)$, for each time step, t , in a set of grid points, (x_i, y_i) . The EOF analysis generates a set of spatial modes, $M_n(x_i, y_i)$ and associated principal components, $h_n(t)$, such that:

$$h(x_i, y_i, t) = \langle h_i \rangle + \sum_n M_n(x_i, y_i) \cdot h_n(t) \quad (\text{S1})$$

where $\langle h_i \rangle$ is the temporal average of $h(x_i, y_i, t)$ in grid point (x_i, y_i) and the index, n , ranges from 1 up to the total number, N , of spatial grid points. If all the modes are included in the sum in Eq. (S1), the expression is exact, but the modes are organized so that the fraction of variance that they explain decreases with n . Thus, the first few modes may often explain most of the variance of $h(x_i, y_i, t)$. This is illustrated in Fig. S1.

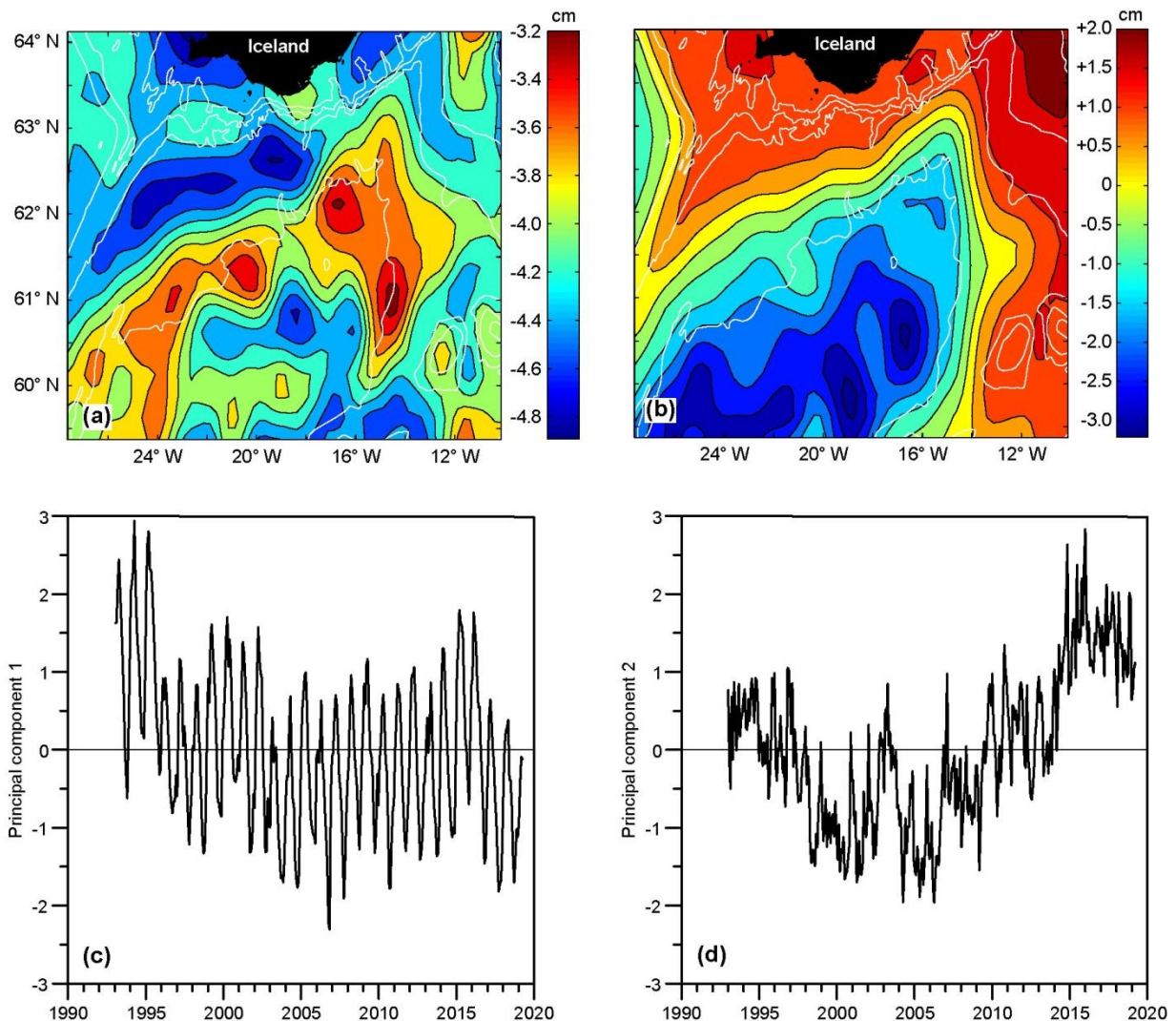


Figure S1. The first two EOF modes of 28-day averaged “unmodified” sea level height from satellite altimetry. (a) Spatial structure of the first mode (explaining 67% of the variance) with depth contours (white lines) for 200 m, 500 m, 1000 m, and 2000 m. (b) Spatial structure of the second mode (explaining 9% of the variance). (c) Principal component of the first mode. (d) Principal component of the second mode.

To reduce the influence from SLA variations in areas outside the region of interest, the spatial grid has been chosen to include only the northern part of the Iceland Basin and its eastern and western boundaries. We define the dimension (cm) to be associated with the spatial modes. The principal components are then dimensionless and are furthermore normalized so that their standard deviations are set to 1 and the spatial modes adjusted accordingly.

As seen in Fig. S1, the first EOF mode of the raw (unmodified) SLA values has the same sign in all the spatial grid points and its principal component is dominated by seasonal and long-term variations. Since the geostrophic surface velocity is determined by the slope of the surface rather than its height, this analysis is not very useful. For the analyses in the main manuscript, we therefore use a set of “modified” SLA values, $h'(x_i, y_i, t)$, where the spatial average is subtracted at each time step:

$$h'(x_i, y_i, t) \equiv h(x_i, y_i, t) - \frac{1}{N} \cdot \sum_i h(x_i, y_i, t) \quad (\text{S2})$$

Absolute Dynamic Topography. In theory, the geostrophic surface flow at a certain time ought to be given by the Absolute Dynamic Topography (ADT), which is the sum of the Mean Dynamic Topography (MDT) and the Sea Level Anomaly (SLA) at the time (Fig. S2).

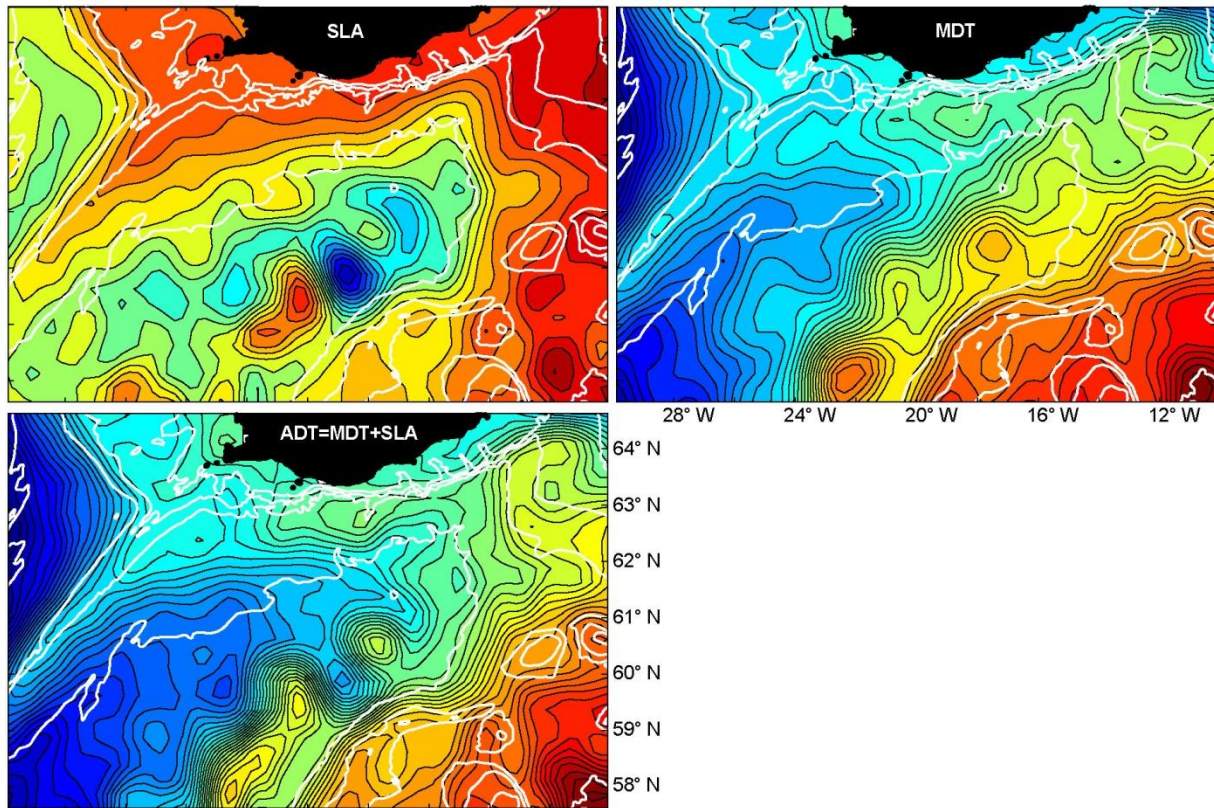


Figure S2. Satellite altimetry for the period from March 2015 to April 2016 showing the Sea level Anomaly (SLA) averaged over the period (top left), the Mean Dynamic Topography (MDT, top right), and the sum of both (bottom). White lines indicate bottom depth 200 m, 500 m, 1000 m, and 2000 m. The colour scales in the three panels are different.

Comparison of altimetry data with direct current measurement in the Iceland-Faroe region has indicated that variations of SLA do reflect near-surface velocity variations with fairly high accuracy when averaged over monthly time scales or longer (Hansen et al., 2018; 2019). The MDT also appears fairly accurate on large spatial scales, but not on small scales (Hansen et al., 2015).

From these results, it is not obvious that the average ADT for a given period gives a more realistic representation of the flow south of Iceland during that period than the average SLA for the period. This is illustrated in Fig. S2, which shows three different aspects of the average sea surface topography during a period when the principal component of the first EOF mode of “modified” SLA was high (Fig. 3d in the main manuscript).

According to the ADT (bottom panel in Fig. S2), there is not an average flow from the Icelandic shelf/slope region towards the southwest into the Iceland Basin in this period. The ADT is seen to be dominated by the MDT in this region and there is little similarity between the average ADT and the average SLA in the period. If the ADT in Fig. S2 is realistic then the SLA only represents the anomalous flow; not the actual flow. In that case, it seems strange that it follows the bottom topography so well. Taking into account that the surface flow tends to follow bottom contours (Taylor–Proudman theorem), the flow associated with the SLA in Fig. S2 seems more realistic than the flow associated with the ADT in the figure.

Thus it seems likely that the MDT and ADT are not sufficiently accurate in the shelf/slope region south of Iceland to represent the actual flow, which is not surprising when the proximity to land and steep bottom topography are considered.

Wind forcing. In order to investigate the ability of the wind to force any one of the EOF modes of the SLA, it may be useful to express the surface air pressure field as a superposition of these modes. To do that, we note that the word “Orthogonal” in “Empirical Orthogonal Function” means that the spatial modes are designed to be orthogonal to one another:

$$\sum_i M_m(x_i, y_i) \cdot M_n(x_i, y_i) = 0 \quad \text{when } n \neq m \quad (\text{S3})$$

so that the complete set of modes forms an orthogonal basis for the vector space containing all the functions on the same spatial grid. This implies that the surface air pressure anomaly (deviation from mean), $p(x_i, y_i, t)$, can be decomposed into the same modes:

$$p(x_i, y_i, t) = \sum_n M_n(x_i, y_i) \cdot p_n(t) \quad (\text{S4})$$

where $p_n(t)$ is a weighting function that determines how strongly each spatial mode is represented in the pressure field at any given time. We are especially interested in the weighting function associated with the first mode and the orthogonality of the modes, Eq. (S3), implies that it is given by:

$$p_1(t) = \frac{\sum_i M_1(x_i, y_i) p(x_i, y_i, t)}{\sum_i M_1(x_i, y_i) \cdot M_1(x_i, y_i)} \quad (\text{S5})$$

To use Eq. (S5), the surface air pressure and the SLA-EOF mode have to be expressed in the same spatial grid. The ERA5 surface air pressure grid has the same resolution as the altimetry grid, but shifted so that each pressure grid point is surrounded equidistantly by four altimetry grid points. The values of $M_I(x_i, y_i)$ were therefore re-gridded to the pressure grid by averaging the values at each of the surrounding four points in the original altimetry grid (Fig. S3). To avoid influence from wind over land or outside the Iceland Basin, the grid points in these areas were excluded in Eq. (S5) by setting $M_I(x_i, y_i)$ to zero in these points.

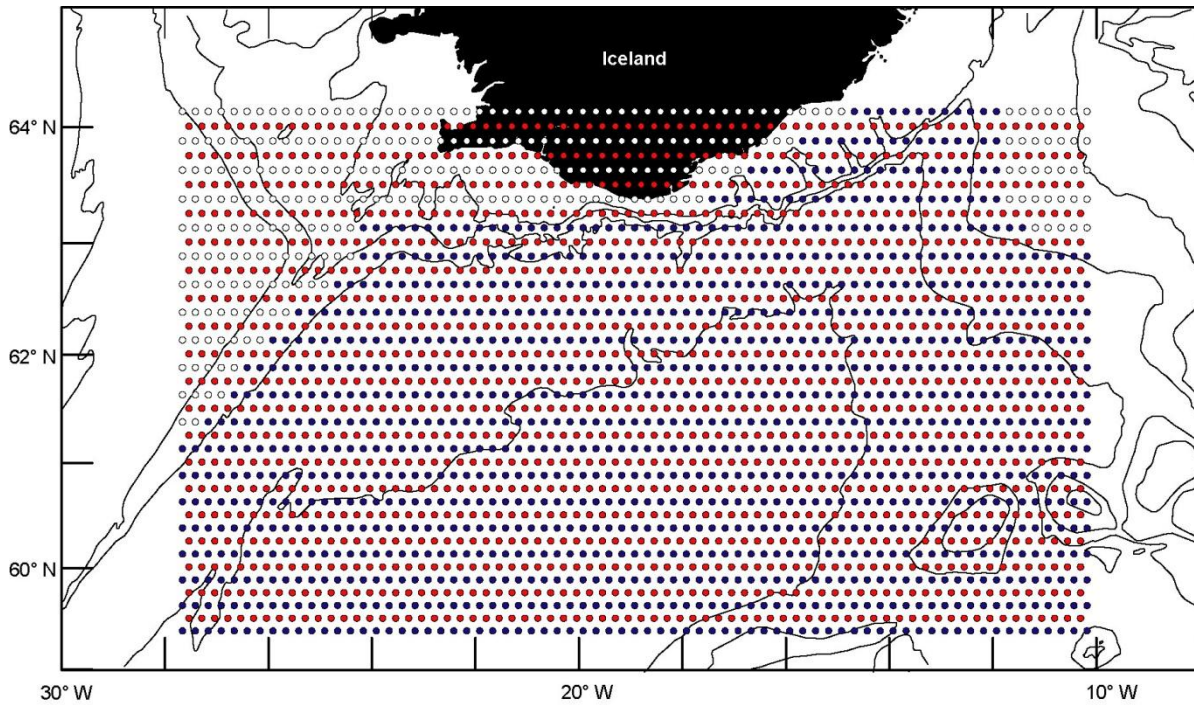


Figure S3. The grid points of the surface air pressure data are marked by red circles. The values of the first (spatial) EOF mode of SLA, $M_1(x_i, y_i)$, are defined in the altimetry grid and marked by the blue circles. The white circles indicate grid points where $M_1(x_i, y_i)$ has been set to zero.

Supplementary methods references

- Hansen, B., Larsen, K. M. H., Hátún, H., Kristiansen, R., Mortensen, E., and Østerhus, S. (2015). Transport of volume, heat, and salt towards the Arctic in the Faroe Current 1993–2013. *Ocean Sci.* 11, 743–757. doi:10.5194/os-11-743-2015.
- Hansen, B., Larsen, K. M. H., Olsen, S. M., Quadfasel, D., Jochumsen, K., Østerhus, S. (2018). Overflow of cold water across the Iceland-Faroe Ridge through the Western Valley. *Ocean Sci.* 14, 871-885. doi.org/10.5194/os-14-871-2018.
- Hansen, B., Larsen, K. M. H., and Hátún, H. (2019). Monitoring the velocity structure of the Faroe Current. Havstovan Technical Report 19-01. www.hav.fo/PDF/Ritgerdir/2019/TechRep1901.pdf.

Supplementary figures

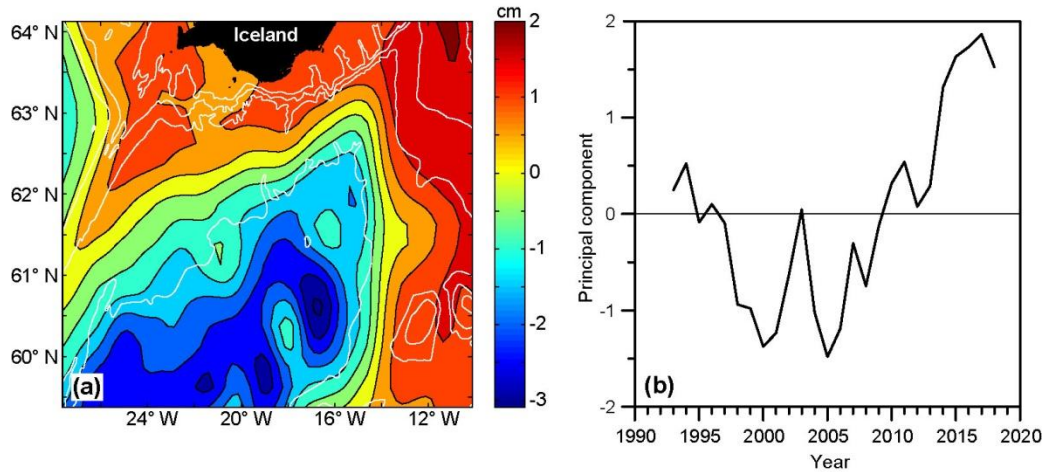


Figure S4. The first EOF mode of 365-day averaged “modified” sea level height from satellite altimetry, $h'(x,y,t)$, explaining 56% of the variance. **(a)** Spatial structure of the mode with depth contours (white lines) for 200 m, 500 m, 1000 m, and 2000 m. **(b)** Principal component.

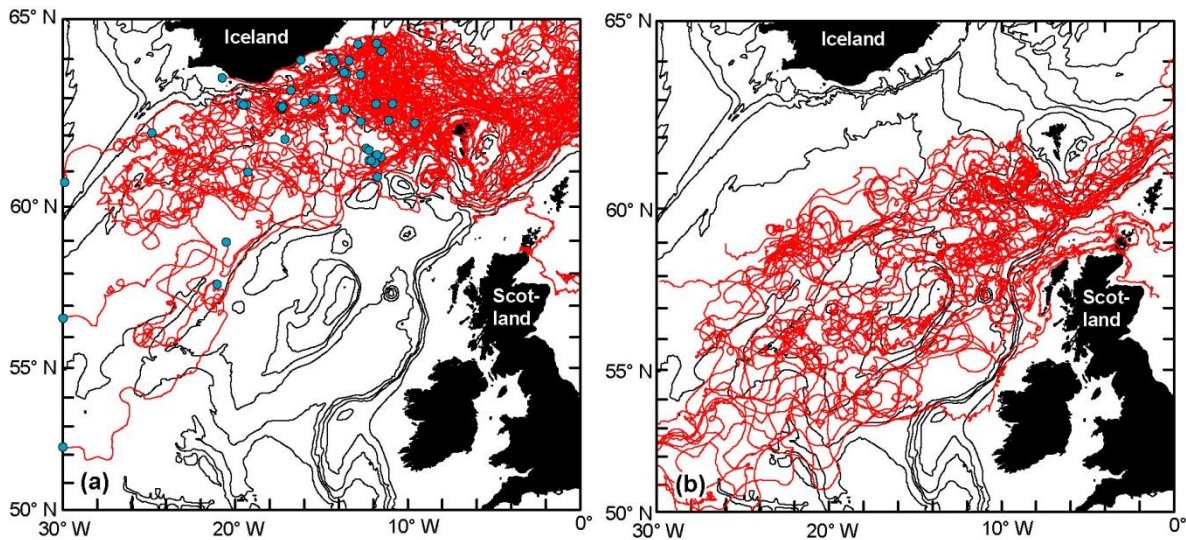


Figure S5. Tracks (red curves) of all the drifters passing eastwards between Iceland and Scotland. **(a)** Drifters entering the Norwegian Sea across the Iceland-Faroe Ridge. Cyan circles indicate position of deployment or where on the boundary the drifter entered the area and show that most of these drifters were deployed within the Iceland Basin. **(b)** Drifters passing south of the Faroes.

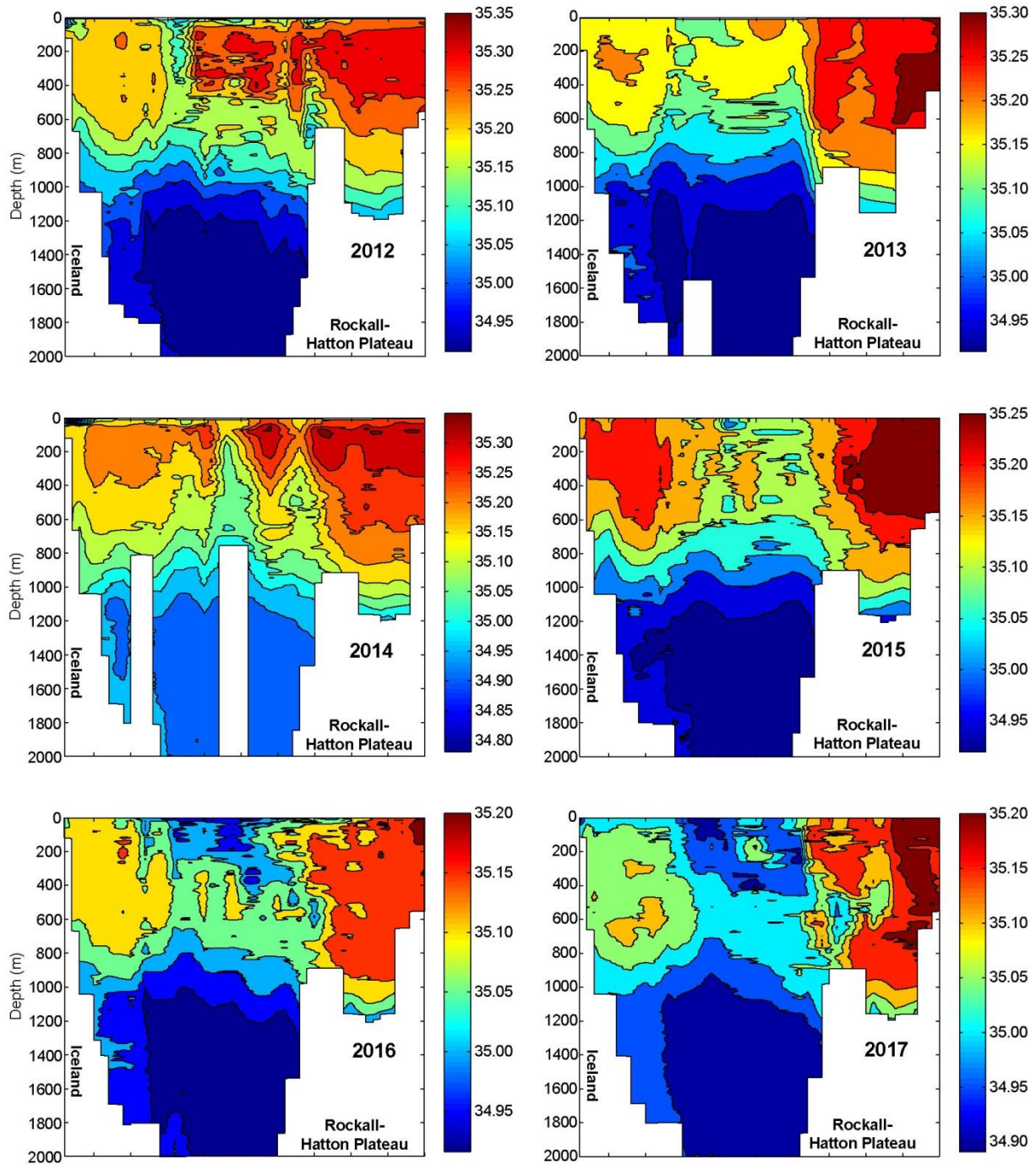


Figure S6. Salinity on the Extended Ellett Line across the Iceland Basin from six annual cruises 2012–2017. All of the cruises were in the May–August period.

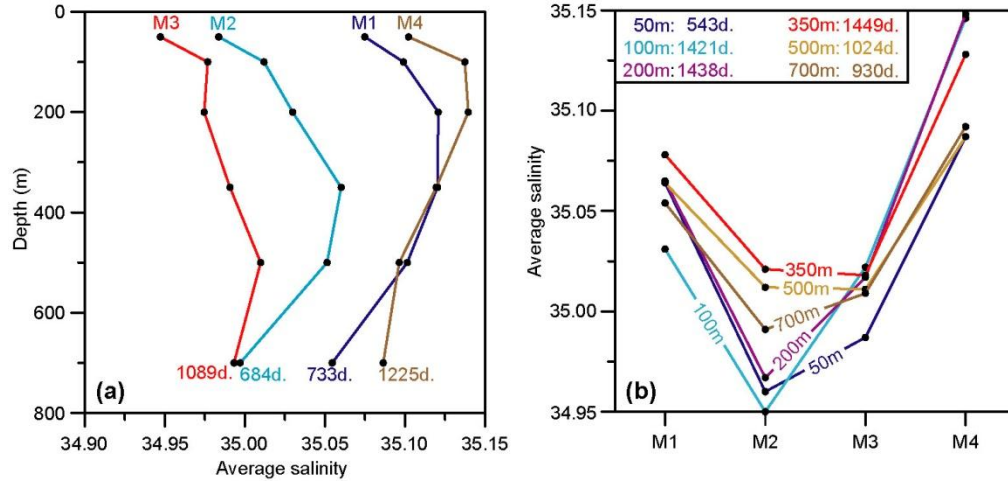


Figure S7. Average salinity at the six uppermost measuring depths at the four OSNAP moorings. (a) Average salinity plotted against depth for each mooring separately. Only days with acceptable data at all six depths are included for each mooring and the number of days (d.) is indicated below each profile. (b) Average salinity plotted against mooring id for each depth separately. Only days with acceptable data at all four moorings are included for each depth and the number of days (d.) is indicated in the top left corner.

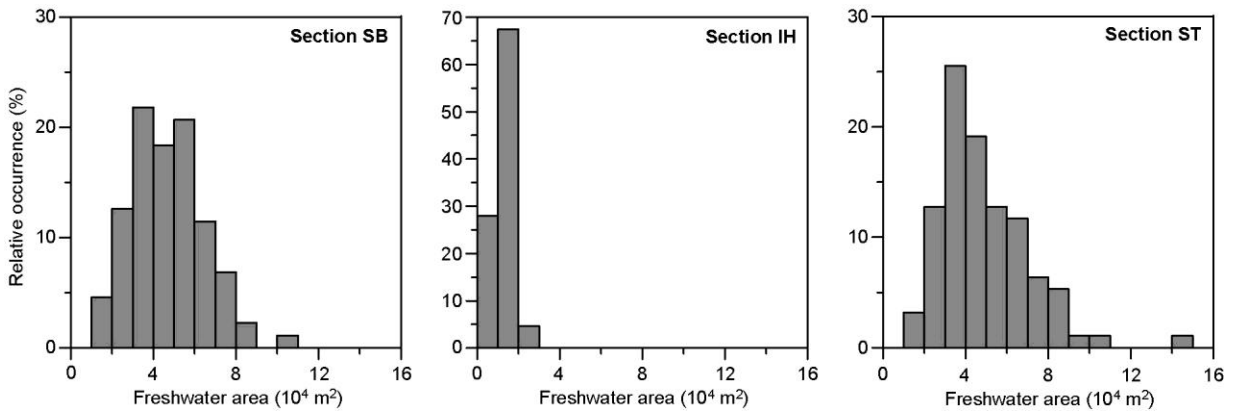


Figure S8. Histograms of freshwater area at the three Icelandic standard sections (Fig. 7a in the main manuscript).

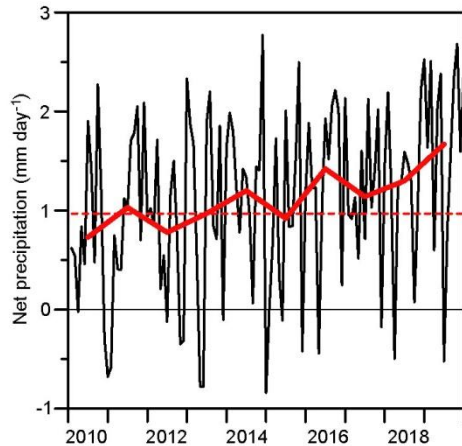


Figure S9. Monthly (black line) and annually (thick red line) averaged net precipitation over the area 55° N – 60° N , 30° W – 20° W from the ERA5 data base. The dashed red line is the overall average for the 1993–2019 period.

Supplementary tables

Table S1. Bottom depths (m) at the thirteen standard stations on the three Icelandic standard sections.

Section SB					Section IH			Section ST				
SB1	SB2	SB3	SB4	SB5	IH1	IH2	IH3	ST1	ST2	ST3	ST4	ST5
46	90	155	510	1021	72	90	108	84	141	216	546	1192

Table S2. Characteristics of the 11 surface drifters that passed from the ISS-region in Fig. 4 in the main manuscript into the “Western Iceland Basin” as defined in the figure. “Entry date” is the date of entry into the Western Iceland Basin. “T-in” is the travel time from entry to (or deployment in) the ISS-region until entry into the Western Iceland Basin. “T-so” is the travel time from entry to (or deployment in) the ISS-region until reaching the southernmost location the Western Iceland Basin, which is listed in the last two columns.

Entry date	T-in	T-so	Southernmost location	
yyyy-mm-dd	Days	Days	Latitude	Longitude
1995-10-26	136	334	58.899° N	29.604° W
1996-12-02	46	50	61.958° N	22.260° W
1996-10-07	18	18	61.959° N	18.054° W
1996-04-03	22	71	58.768° N	24.854° W
1997-07-07	18	44	60.623° N	20.478° W
1999-07-19	74	289	58.935° N	25.877° W
2013-09-17	74	78	61.957° N	19.455° W
2014-04-07	38	59	61.270° N	20.552° W
2015-01-16	56	57	61.986° N	16.397° W
2015-07-19	97	124	61.277° N	24.040° W
2018-10-04	51	73	61.574° N	20.174° W

Table S3. Number of days from October to June each winter, for which the difference in potential density between 50 m depth and the other instrumented depths above 500 m is less than 0.01 kg m^{-3} for at least 12 of the 48 daily measurements at each of the OSNAP sites. Data missing at either 50 m or one of the other depths is indicated by a minus sign.

Depth (m):	M1				M2				M3				M4			
	100m	200m	350m	500m												
2014-2015	226	156	102	45	162	127	97	36	122	86	33	-	189	112	24	3
2015-2016	156	131	92	37	117	20	2	0	160	43	0	0	157	56	1	0
2016-2017	-	-	-	-	-	-	-	-	145	32	0	0	151	73	3	0
2017-2018	-	-	-	-	-	-	-	-	157	57	27	0	158	92	37	1

Table S4. Number of days from October to June each winter, for which the difference in potential density between 100 m depth and the other instrumented depths above 500 m is less than 0.01 kg m^{-3} for at least 12 of the 48 daily measurements at each of the OSNAP sites. Data missing at either 100 m or one of the other depths is indicated by a minus sign.

Depth (m):	M1			M2			M3			M4		
	200m	350m	500m									
2014-2015	172	107	43	110	89	38	115	38	-	137	34	5
2015-2016	147	103	39	51	4	0	62	0	0	100	3	0
2016-2017	130	79	15	46	0	0	61	0	0	110	3	0
2017-2018	137	62	6	91	10	0	69	28	0	114	42	2